Sensitivity Analysis of Aero-Propulsive Coupling for Over-Wing-Nacelle Concepts

Steven H. Berguin*, Sudharshan Ashwin Renganathan†, Jai Ahuja †,
Mengzhen Chen†, Jimmy Tai *, Dimitri N. Mavris‡
Georgia Institute of Technology, Atlanta, GA, 30332, USA
and
David P. Hills§
Airbus Americas Inc, Herndon, VA, 20171, USA

A sensitivity analysis is performed to quantify the relative impact of perturbing a set of design variables representing an airplane configuration with Over-Wing Nacelles (OWN), operating at transonic cruise. The goal is to study the impact of perturbing the engine's XYZ position and power setting on installation drag, engine inlet pressure recovery, and lift curve characteristics. High-fidelity Reynolds Averaged Navier-Stokes (RANS) simulations of the Common Research Model (CRM) modified with powered, over-wing nacelles are performed and dominant *main effects* and *interactions* are identified. The most dominant effect was by far the engine's X position, but it was also found that podded OWN configurations exhibit statistically significant, aero-propulsive coupling. Specifically, certain engine locations cause changes in the flow-field that deteriorate inlet pressure recovery and, vice versa, a change in engine boundary conditions can affect installation drag. It is therefore recommended to simulate OWN concepts using a coupled MDA or MDAO approach to capture interdependencies between aerodynamics and propulsion.

I. Introduction

Numerical Propulsion-Airframe Integration (PAI) studies usually adopt a decoupled solution method, in which the effect of the engine on the flow field is accounted for through the application of powered boundary conditions in CFD, but the effect of airframe aerodynamics on the engine is not. The need to account for such coupling is obvious for certain applications like Boundary Layer Ingestion (BLI) engines,[1] but perhaps less so for podded nacelle configurations such as Over-Wing Nacelles (OWN) concepts. The development of OWN such as the Boeing YC-14[2] is historically tied to Upper Surface Blowing (USB) technology for Short Takeoff and Landing (STOL) applications where leading-edge, slipper-mounted engines generate powered lift by blowing hot exhaust over the top surface of the wing to take advantage of the Coandă effect; a highly coupled, multi-disciplinary problem. However, modern applications such as the Lockheed HWB[3] have shifted the paradigm from "design for STOL" to "design for energy efficiency" using trailing-edge, podded engines configuration, likely to exhibit weaker aero-propulsive coupling; but how much weaker? The purpose of this paper is to quantify the strength of aero-propulsive coupling for podded OWN. This will be accomplished using statistical analysis to quantify the sensitivity of powered effects on installation drag, engine pressure recovery, and lift curve characteristics at cruise as a function of nacelle XYZ location and power setting. All data is generated using the Reynolds Averaged Navier-Stokes (RANS) equations with a validated CFD model of the NASA Common Research Model[4] (CRM), modified with over-wing engines. The rest of the paper is organized as follows: the next section describes the general methodology used for

*Research Engineer II, School of Aerospace Engineering, AIAA Member.
†PhD Candidate, Aerospace Systems Design Laboratory, and AIAA Student Member.
‡Boeing Professor of Advanced Aerospace Systems Analysis, School of Aerospace Engineering, AIAA Fellow
§VP Research & Technology at Airbus Americas Inc, AIAA Member

sensitivity analysis, followed by a more specific description of the experiment, CFD modeling and simulation setup with validation, results, and conclusions.

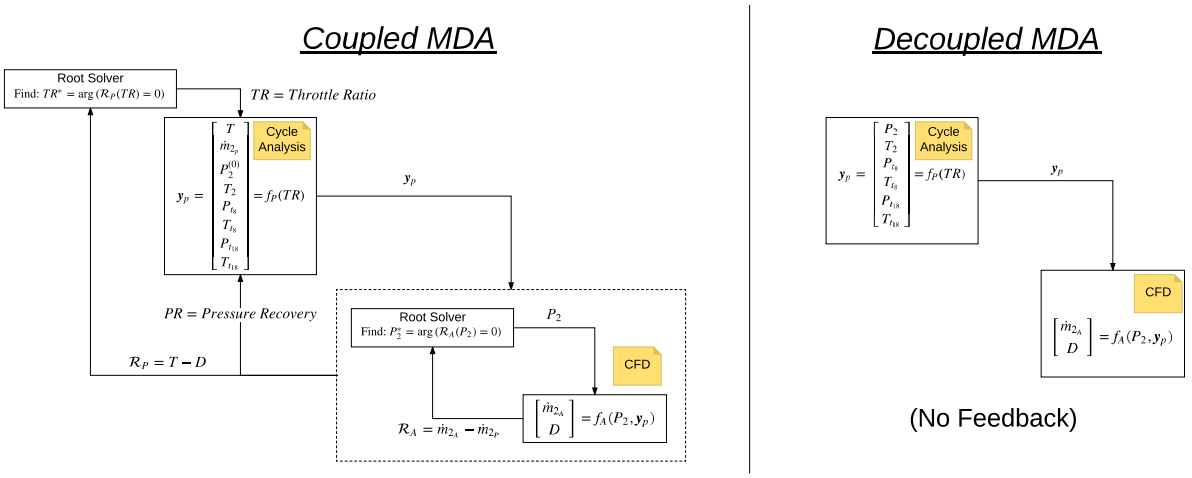

Figure 1: Illustration of coupled *vs.* decoupled Multi-Disciplinary Analysis (MDA) for PAI. *One the left, there is both feedback and feed-forward between the contributing analyses; multi-disciplinary convergence is achieved iteratively using some root solver to minimize some residual, e.g. thrust equals drag ($\mathcal{R}_P^* = T - D = 0$) or predicted mass flow rate equals prescribed mass flow rate ($\mathcal{R}_A^* = \dot{m}_P - \dot{m}_A = 0$). On the right, there is only feed-forward, where y_p denotes the coupling variables from cycle analysis to CFD. They include static properties at the fan face (P_2, T_2) and stagnation properties at the core and bypass nozzle inlets ($P_{t_8}, P_{t_8}, T_{t_{18}}, T_{t_{18}}$).*

II. Mathematical Approach

Multi-Disciplinary Analysis (MDA) captures inter-disciplinary coupling; but it is complex and computationally expensive. Hence, it makes sense to first test for strong inter-disciplinary coupling before deciding to invest the resources. Indeed, one need not solve an MDA to quantify the strength of aero-propulsive coupling; so-called effects screening can be used to that end. The method uses *screening experiments* from the field of Design Of Experiments (DOE), *linear regression*, and *Analysis of Variance* (ANOVA) to test for the significance main effects and two-factor interactions.[5,6] Hence, in order to test for the presence of strong aero-propulsive coupling, it suffices to statistically quantify the significance of any interaction between the two disciplines. If no significant interaction exists, then the coupling is weak. This section explains the theory used to accomplish this following the development by Hines et al.[5]

A. Statistical Analysis

Consider the general linear regression model given by,

$$y = f(\boldsymbol{x}) = \sum_{j=1}^{m} \beta_j \phi_j(\boldsymbol{x}) + \epsilon \quad \text{where} \quad \epsilon \sim \mathcal{N}(0, \sigma^2) \tag{1}$$

where $f \in \mathbb{R}$ is some deterministic function of interest, $\boldsymbol{x} \in \mathbb{R}^p$ is a vector of standardized design variables, β_j are unknown regression coefficients to be found and ϕ_j is some assumed basis function associated with the j^{th} coefficient. This model assumes that the residual error ϵ is Gaussian. This error could be the result of true random variation in a stochastic process or, small deterministic error that appears random due to the assumed form of the model (*i.e.* the assumed model does not exactly capture the response but it is close), or both. The magnitudes of the coefficients β_j are indicative of the relative importance of a given

basis function ϕ_j. Consider a dataset of N samples,

$$\begin{pmatrix} y_1 \\ \vdots \\ y_N \end{pmatrix} = \begin{pmatrix} \phi_1(\boldsymbol{x}_1) & \dots & \phi_m(\boldsymbol{x}_1) \\ \vdots & \ddots & \vdots \\ \phi_1(\boldsymbol{x}_N) & \dots & \phi_m(\boldsymbol{x}_N) \end{pmatrix} \begin{pmatrix} \beta_1 \\ \vdots \\ \beta_m \end{pmatrix} \quad \Leftrightarrow \quad \boldsymbol{y} = \boldsymbol{X}\boldsymbol{\beta} \tag{2}$$

where $\boldsymbol{y} \in \mathbb{R}^N$, $\boldsymbol{X} \in \mathbb{R}^{N \times m}$ and $\boldsymbol{\beta} \in \mathbb{R}^m$. Under the standard setting where $N > m$, the solution to Eq. 2 is usually obtained using the Least Squares Estimator (LSE):

$$\hat{\boldsymbol{\beta}} = \arg\min_{\boldsymbol{\beta} \in \mathbb{R}^m} L \quad \text{where} \quad L = (\boldsymbol{y} - \boldsymbol{X}\boldsymbol{\beta})'(\boldsymbol{y} - \boldsymbol{X}\boldsymbol{\beta}) = \sum_{i=1}^{N} \left(y_i - \sum_{j=1}^{m} \beta_j \phi(x_{ij}) \right)^2 \tag{3}$$

This can be solved in two ways: optimization or using the normal equations. Using the latter, taking the partial derivatives with respect to β_j, and setting to zero, one obtains a linear system of m equations:

$$\left. \frac{\partial L}{\partial \boldsymbol{\beta}} \right|_{\hat{\boldsymbol{\beta}}} = -2\boldsymbol{X}'\boldsymbol{y} + 2\boldsymbol{X}'\boldsymbol{X}\hat{\boldsymbol{\beta}} = \boldsymbol{0} \tag{4}$$

The solution to these normal equations is given by:

$$\hat{\boldsymbol{\beta}} = (\boldsymbol{X}'\boldsymbol{X})^{-1}\boldsymbol{X}'\boldsymbol{y} \tag{5}$$

1. Statistical Properties

Note that the least squares estimator in Eq. 5 is a random vector, since ϵ is Gaussian,

$$\hat{\boldsymbol{\beta}} = (\boldsymbol{X}'\boldsymbol{X})^{-1}\boldsymbol{X}'(\boldsymbol{X}\boldsymbol{\beta} + \epsilon) \tag{6}$$

and, moreover, it is Gaussian itself since a linear combination of Gaussian terms is still Gaussian. Applying definitions of mean and covariance, it can be shown that $\hat{\boldsymbol{\beta}}$ is an unbiased estimator of $\boldsymbol{\beta}$, with parameters:

$$\mathbb{E}(\hat{\boldsymbol{\beta}}) = \boldsymbol{\beta} \tag{7}$$

$$\mathrm{Cov}(\hat{\boldsymbol{\beta}}) = \sigma^2(\boldsymbol{X}'\boldsymbol{X})^{-1} \tag{8}$$

It is necessary to estimate σ^2. To do so, re-write the sum of squares of the residuals in Eq. 3 as:

$$SS_E = |\boldsymbol{y} - \boldsymbol{X}\boldsymbol{\beta}|_2^2 = (\boldsymbol{y} - \boldsymbol{X}\hat{\boldsymbol{\beta}})'(\boldsymbol{y} - \boldsymbol{X}\hat{\boldsymbol{\beta}}) = \boldsymbol{y}'\boldsymbol{y} - \hat{\boldsymbol{\beta}}'\boldsymbol{X}'\boldsymbol{y} \tag{9}$$

All the terms in this equation are known, since they can be calculated from the data. There are $N - m$ degrees of freedom, which represents the number of data samples available beyond the minimum necessary. Hence, the mean square error is given by:

$$MS_E = \frac{SS_E}{N - m} \tag{10}$$

Others have shown that the expected value of MS_E is σ^2; hence, an unbiased estimator of σ^2 is given by

$$\hat{\sigma}^2 = MS_E \tag{11}$$

2. Hypothesis Testing on Individual Regression Coefficients

The hypotheses for testing the significance of any individual regression coefficient β_j is:

$$\text{H0:} \quad \beta_j = 0, \tag{12}$$

$$\text{H1:} \quad \beta_j \neq 0. \tag{13}$$

Recall that individual coefficients are distributed as $\hat{\beta}_j \sim \mathcal{N}(\beta_j, \sigma^2 C_{jj})$ where C_{jj} is the diagonal element of $(\boldsymbol{X}'\boldsymbol{X})^{-1}$ in Eq. 7. Hence, under the null hypothesis, the quantity t_0 follows a student-t distribution:

$$t_0 = \frac{\hat{\boldsymbol{\beta}}_{\boldsymbol{j}}}{\sqrt{\hat{\sigma}^2 C_{jj}}} \tag{14}$$

The null hypothesis H0: $\beta_j = 0$ would thus be rejected at the $1-\alpha$ confidence level if $|t_0| > t_{\alpha/2,N-m}$. Alternatively, this result is often expressed as a p-value, which expresses the probability that the observed value of t_0 is greater than what it should be under the null hypothesis:

$$p = P\left(|t_0| > t_{\alpha/2,N-m} | H0\right) \tag{15}$$

If $p \leq 0.05$, then this is usually a strong indicator that β_j is statistically significant; otherwise, it can be dropped from the model. In the case of effects screening, where β_j multiplies main effects x_j, the latter implies that x_j contributes little to the response and can thus be defaulted to some fixed value. Once t_0 has been established for each coefficient, the "vital few" can be separated from the "trivial many." One popular method is Lenth's Pseudo Standard Error (PSE),[7] which describes a repeatable process for determining the decision threshold; the reader is referred to the literature for more detail.

B. Concept Behind Effects Screening

With this background in place, the concept behind effect screening can now be explained. It proceeds by sampling the extremes of the design space, using specialized sampling plans known as screening designs, followed by statistical regression. The idea is to choose the basis functions ϕ_j such that they are functions of only specific design variables (i.e. $\phi_j(\boldsymbol{x}) = \phi_j(x_j)$). In the methods by Myers and Montgomery,[8] the basis functions are taken to form a linear model containing main effects and two-factor interactions only,

$$f = \beta_0 + \underbrace{\sum_{i=1}^{p} \beta_i x_i}_{\text{main effects}} + \underbrace{\sum_{i=1}^{p-1} \sum_{j=i+1}^{p} \beta_{ij} x_i x_j}_{\text{two-factor interactions}} \tag{16}$$

As a result, the magnitude of the coefficients β_i indicate the relative importance of the main effects x_i and β_{ij} indicate the relative importance of the two-factor interactions $x_i x_j$. Higher-order interactions are neglected under the sparsity-of-effects principle (also known as the Pareto principle), which is based on the observation that in most engineering problems the response is only driven by a small number of main effects and second-order interactions.[8]

1. *Constructing the Sampling Plan*

Up to now, the methodology has explained how to use a given set of data in order to draw conclusions about the importance of main effects; but how should this data be generated in the first place? Screening designs stem from the field of designs of experiment. They seek to maximize information about the design space, while minimizing the number of samples needed for an assumed statistical model. For instance, the minimum number of samples needed to regress Eq. 16 is obtained by counting the number of regression coefficients β:

$$N_{min} = 1 + p + p(p-1)/2 \tag{17}$$

For large design spaces ($p \gg 10$), this number can be large, which defeats the purpose of screening. However, it can be reduced if terms are grouped together in a concept known as aliasing.[8] For example, a three-variable model can be reduced from $2^3 = 8$ coefficients to $2^{3-1} = 4$ by aliasing main effects and two-factor interactions:

$$f = \beta_0 + \beta_1 \underbrace{(x_1 + x_2 x_3)}_{\text{aliased}} + \beta_2 \underbrace{(x_2 + x_1 x_3)}_{\text{aliased}} + \beta_3 \underbrace{(x_3 + x_1 x_2)}_{\text{aliased}} \tag{18}$$

The only disadvantage is that it is no longer possible to tell main effects x_i apart from two-factor interactions $x_j x_k$, since the magnitude of β_j only provides information about the group $x_i + x_j x_k$. The ability to distinguish main effects apart from interactions is a property known as resolution.[8] It is determined by the sampling plan, which are typically chosen to be fractional factorial designs of resolution III and IV[8] or Plackett-Burman designs:[9]

- **Resolution III designs** are designs in which no main effects are aliased with any other main effect, but main effects are aliased with two-factor interactions, and two-factor interactions may be aliased with each other.
- **Resolution IV designs** are designs in which no main effects are aliased with any other main effect or with any two-factor interaction, but two-factor interactions may be aliased with each other.
- **Resolution V designs** are designs in which no main effects or two-factor interactions are aliased with any other main effect or with any two-factor interaction.

An example of a resolution IV fractional factorial design is given in Table 1. Treatments $\tau_1, \ldots, \tau_8$ represent the full factorial, whereas treatments $\tau_1, \ldots, \tau_4$ represent the fractional factorial. As can be seen, these types of screening designs assume only two levels for each factor, denoted by the "+" and "−" symbols, corresponding to the maximum ($x_{i,max}$) and minimum ($x_{i,min}$) bounds of the design space, respectively. Skipping over much of the theory behind design of experiments, this design yields the following alias structure,

$$x_1 = x_2 x_3 \qquad x_2 = x_1 x_3 \qquad x_3 = x_1 x_2 \tag{19}$$

which agrees with Eq. 18. In other words, treatments $\tau_1, \ldots, \tau_4$ in Table 1 is the minimum screening design required to regress Eq. 18.

Table 1: Example of a 2^{3-1} factorial design

Treatment No.	x_1	x_2	x_3	y
τ_1	+	+	−	$y^{(1)}$
τ_2	+	−	+	$y^{(2)}$
τ_3	+	−	−	$y^{(3)}$
τ_4	+	+	+	$y^{(4)}$
τ_5	+	+	+	$y^{(5)}$
τ_6	+	+	−	$y^{(6)}$
τ_7	+	−	+	$y^{(7)}$
τ_8	+	−	−	$y^{(8)}$

Note that if one wished to resolve all terms, as in Eq. 20, then one would have to run the full factorial $\tau_1, \ldots, \tau_8$. Adding more data always increases resolution, but care must be taken to keep the design balanced. Mathematically, this means there must always be an equal number of "+" and "−" in each column of Table 1. In other words, this means that for a given design resolution, the model must not be biased due to uneven sampling of the design space. Hence, increasing resolution is always achieved by "folding over" the design, as illustrated in Table 1, which increases the number of runs required by a factor of two every time.

$$f = \beta_0 + \beta_1 x_1 + \beta_2 x_2 + \beta_3 x_3 + \beta_{23} x_{23} + \beta_{13} x_{13} + \beta_{12} x_{12} \tag{20}$$

III. Design of Experiment

Now that the general theory behind *effect screening* in place, it can be applied to the problem at hand. The factors, responses, and design of experiment selected for this study are shown in Table 2, where the raw data used for analysis in Section V has been included. The DOE consists of a fractional factorial design of resolution V augmented with baseline runs, where each treatment $(\tau_1, \ldots, \tau_{22})$ was evaluated using the modeling and simulation environment described in section IV. The following subsections will now define the quantities associated with each column in Table 2.

A. Definition of Factors

The five factors are the relative nacelle displacements (ΔX, ΔY, ΔZ), configuration type, and engine Power Code (PC). Their definitions are provided in Fig. 2. For convenience, a distinction was made between

Table 2: Raw data at $C_L = 0.5$, M= 0.85, $alt = 10,668\ m$ ($c = 7.96\ m,\ w = h = 3.80\ m$). *In order to match C_L, each case was run at $\alpha = \{0, 2, 4\}$ deg from which linear regression was used to find C_{L_α}, C_{L_0}, α_{match}.*

Treatment	$\Delta X/c$	$\Delta Y/w$	$\Delta Z/h$	Config	PC	ΔC_{L_α}	ΔC_{L_0}	ΔC_D	ΔPR
	–	–	–	–	–	$10^{-4} \cdot deg^{-1}$	10^{-4}	10^{-4}	%
τ_1	−0.20	−0.35	0.30	LE	50	-110	80.0	19	2.00
τ_2	+0.30	+0.35	0.00	TE	50	140	-1140	32	0.91
τ_3	+0.30	−0.35	0.00	LE	50	-280	-910	357	0.07
τ_4	−0.20	−0.35	0.00	TE	50	80	-1980	269	2.27
τ_5	−0.20	+0.35	0.00	LE	50	-100	240	16	0.01
τ_6	−0.20	+0.35	0.30	TE	50	-100	-1600	326	0.15
τ_7	+0.30	−0.35	0.30	TE	50	70	-970	21	0.14
τ_8	+0.30	−0.35	0.00	TE	40	130	-1110	21	0.38
τ_9	+0.30	−0.35	0.30	LE	40	-350	-590	36	0.04
τ_{10}	−0.20	+0.35	0.00	TE	40	-220	-1970	406	0.39
τ_{11}	−0.20	−0.35	0.30	TE	40	-50	-2100	305	0.34
τ_{12}	−0.20	−0.35	0.00	LE	40	-260	210	107	0.02
τ_{13}	+0.30	+0.35	0.00	LE	40	-380	-320	300	0.02
τ_{14}	+0.30	+0.35	0.30	LE	50	-430	100	276	0.02
τ_{15}	−0.20	+0.35	0.30	LE	40	60	-20	0	0.00
τ_{16}	+0.30	+0.35	0.30	TE	40	140	-1280	45	0.27
τ_{17}		Baseline		TE	40	120	-2100	99	2.50
τ_{18}		Baseline		TE	44	130	-1960	89	2.29
τ_{19}		Baseline		TE	50	-400	120	77	1.92
τ_{20}		Baseline		LE	40	-410	130	206	0.00
τ_{21}		Baseline		LE	44	-420	170	207	0.05
τ_{22}		Baseline		LE	50	-100	-1600	216	0.00

Leading Edge (LE) and Trailing Edge (TE) configurations such that the Δ's are always expressed relative to a local coordinate system that depends on the configuration type, as shown in Fig. 2a. Note that the local X-axis is reversed for the TE baseline to ensure that $+\Delta X$ is always towards the wing and $-\Delta X$ is always a away from it. Beyond engine displacement, changing the power setting is a way to test the strength of the aero-propulsive coupling. Indeed, if airframe aerodynamics are sensitive to changes in the engine's boundary conditions, then artificially changing the engine's power code is a way to find out; otherwise, the coupling is weak. Fig. 2b shows the baseline engine's power hook and the selected range of power codes (*i.e.* power codes 40 – 50).

B. Definition of Responses

The four responses of interest are: installation drag ΔC_D, change in pressure recovery ΔPR, change in lift curve slope ΔC_{L_α}, and change in lift curve intercept ΔC_{L_0}. This subsection will now define them clearly.

1. Installation Drag

When the engine is brought into close proximity of the wing-body, the flow field of the former interacts with the flow field of the latter, possibly resulting in excess drag beyond that of the isolated bodies. This is termed installation drag and can thus be decomposed into two components: (i) the change in drag on the wing-body due to the presence of a nacelle and (ii) the change in drag on the nacelle due to integration with the wing-body. However, since installing an engine onto a clean wing changes the effective angle of attack, care must be taken to compute installation drag at a constant C_L. In the definition that follows, the notation $(C_{D,x})^y_z$ denotes drag coefficient computed on the surface x (*i.e.* wing-body, nacelle) of the configuration

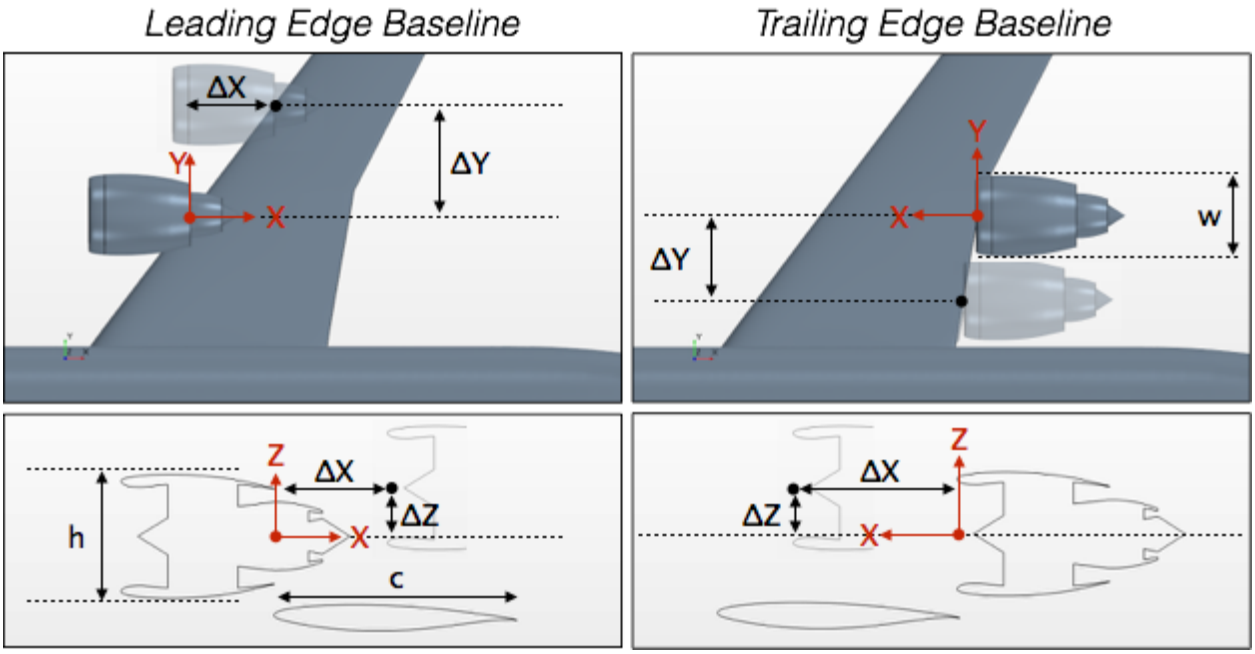

(a) Definition of relative displacements and configuration type

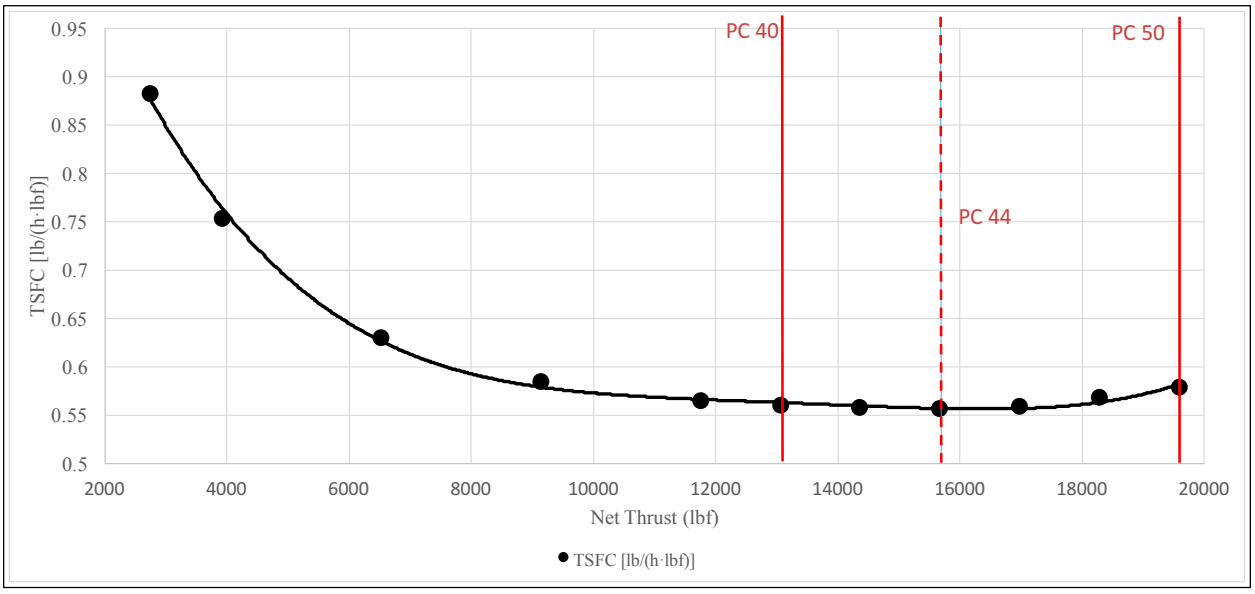

(b) Selected power code range of variation for notional high bypass turbofan of 94,000 lb thrust class

Figure 2: Definition of the factors varied in the experiment

y (*i.e.* wing-body-nacelle, wing-body, isolated-nacelle) at constant z (*i.e.* C_L). The installation drag is denoted by $\Delta\ C_D$ according to:

$$\Delta\left(C_{D_{WB}}\right)_{C_L}^{WBN} = \left(C_{D_{WB}}\right)_{C_L}^{WBN} - \left(C_{D_{WB}}\right)_{C_L}^{WB} \tag{21}$$

$$\Delta\left(C_{D_N}\right)_{C_L}^{WBN} = \left(C_{D_N}\right)_{C_L}^{WBN} - \left(C_{D_N}\right)_{C_L=0}^{N} \tag{22}$$

$$\Delta C_D \equiv \Delta\left(C_{D_{WBN}}\right)_{C_L}^{WBN} = \left(\Delta C_{D_N}\right)_{C_L}^{WBN} + \left(\Delta C_{D_{WB}}\right)_{C_L}^{WBN} \tag{23}$$

2. Inlet Pressure Recovery

The inlet pressure recovery (PR) is defined as the ratio of total pressures at the fan-face (P_{t2}) and the freestream (P_{t0}). Under ideal conditions, this ratio is 1 but non-isentropic losses can cause this number to drop. Let the change in pressure recovery due to engine installation be defined as:

$$\Delta PR = \left(\frac{P_{t2}}{P_{t0}}\right)_{Isolated-N} - \left(\frac{P_{t2}}{P_{t0}}\right)_{WBN} \tag{24}$$

3. Lift Curve Parameters

Let the parameters $C_{L\alpha}$ and C_{L0} denote the lift curve slope and intercept, respectively, and let $(C_{L_x})^y$ denote the parameter x (*i.e.* C_{L_α} or C_{L_0}) computed on the configuration y (*i.e.* wing-body-nacelle or isolated wing-body). The change in parameters due to engine installation is then given by:

$$C_L = C_{L_0} + \alpha\, C_{L\alpha} \tag{25}$$

$$\Delta C_{L_0} = (C_{L_0})^{WBN} - (C_{L_0})^{WB} \tag{26}$$

$$\Delta C_{L_\alpha} = (C_{L_\alpha})^{WBN} - (C_{L_\alpha})^{WB} \tag{27}$$

IV. Modeling and Simulation

The raw data presented in Table 2 was obtained numerically using CFD. This section describes the models and solver used to capture the physics, including validation.

A. Navier-Stokes Solver

All results were generated using the commercial software STAR-CCM+ under fully turbulent, steady-state, Reynolds-Averaged Navier-Stokes (RANS) assumptions. The solver uses a finite volume approach with implicit time integration scheme and 2nd order upwind spatial discretization. The flux at the boundary is reconstructed using Roe flux difference splitting with the Venkatakrishnan limiter. The Courant number was set to 5 and, to accelerate convergence, an Algebraic Multi-Grid (AMG) method was used with 30 V-cycles and a Gauss-Seidel relaxation scheme.

B. Airframe Model

The baseline aircraft is the NASA CRM[4] modified with over-wing nacelles at $C_L = 0.5$, $M = 0.85$, and an altitude of $10,668m$. The pylon and tail are not considered in this study. Known geometry issues[10] with the fuselage fairing and nacelle necessitated minor modifications to repair self-intersecting surfaces and close gaps; however the wing is unchanged. The study was conducted using an unstructured Cartesian mesh, as shown in Figure 3b, augmented with 30 layers of high aspect ratio prism cells near the surface to resolve the boundary layer. Choosing a $y+$ value of 1 resulted in a near wall cell height of $5.34e{-}6$ m. The final mesh contained $\mathcal{O}(24M)$ cells for the Wing-Body (WB) and $\mathcal{O}(30M)$ cells for the Wing-Body-Nacelle (WBN), resulting in a CPU Time per solver iteration of approximately 4 $cpu \cdot min/iteration$ for the wing-body and 5 $cpu \cdot min/iteration$ for the wing-body-nacelle. Model validation is provided in Figure 3a for the wing-body by comparing the computed pressure coefficient distributions with those obtained by Vassberg.[4] Good agreement is observed between the two sets of data.

C. Powered Nacelle Model

The engine was simulated in CFD by imposing flow boundary conditions at the fan-face, bypass nozzle plenum, and core nozzle plenum as shown in Fig. 4. Thermodynamic properties at each of these boundary conditions were obtained from a simulated model of a notional high bypass turbofan of the 94,000 lbs thrust class turbofans sized for a representative twin-aisle mission with a cruise design point of $C_L = 0.5$, $M = 0.85$, and altitude of $10,668\ m$. This engine was selected because it was readily available and the CRM does not have an "official" engine cycle publicly available; only a through-flow nacelle. The engine model was developed (and calibrated) using publicly available information, following a rigorous multi-design point vehicle sizing process known as the Environmental Design Space (EDS).[11] However, there is a limitation: the

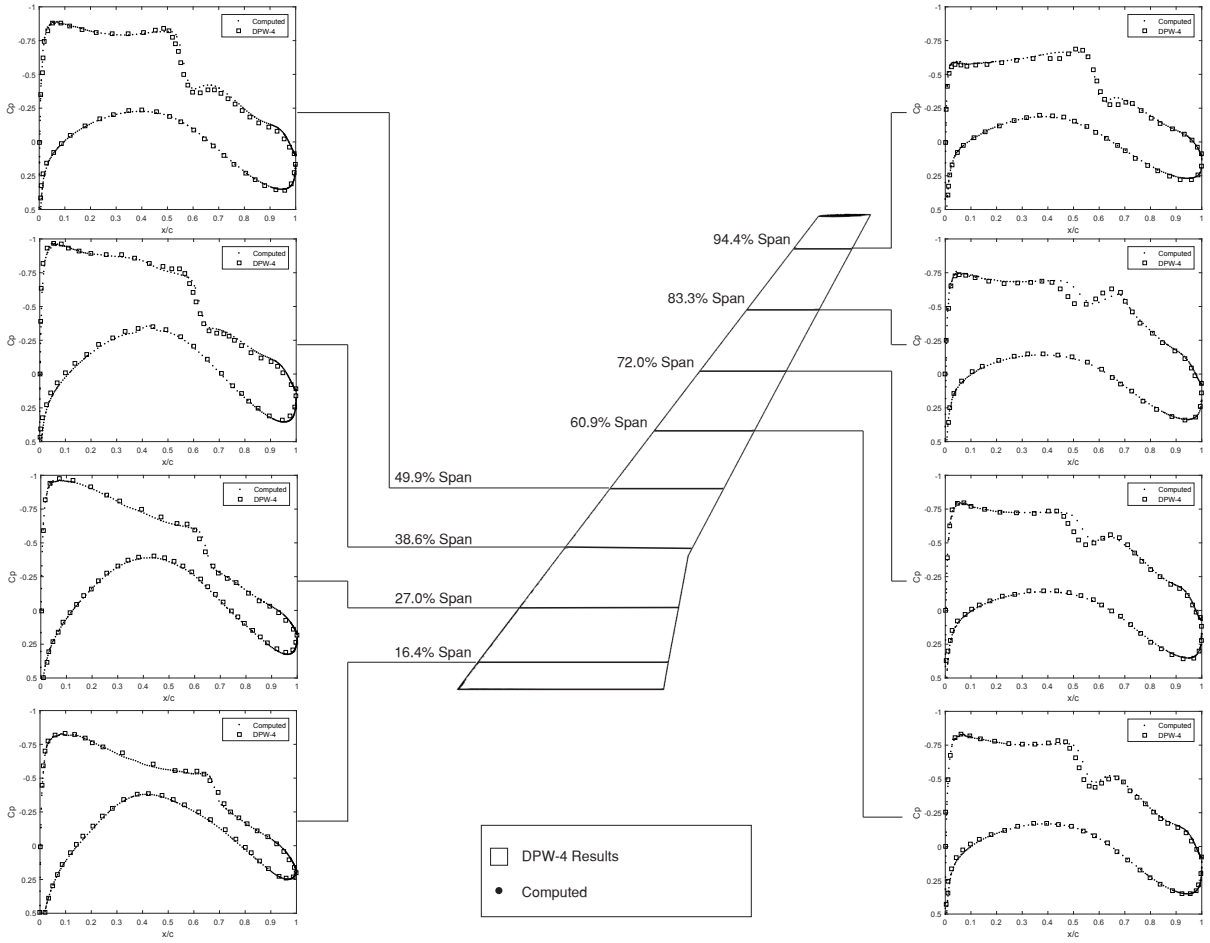

(a) CRM wing-body validation against DPW-4[4]

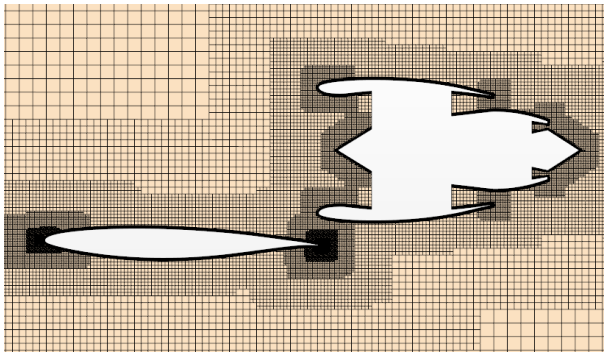

(b) Wing-Body-Nacelle (WBN) mesh – $\mathcal{O}(30M)$ cells

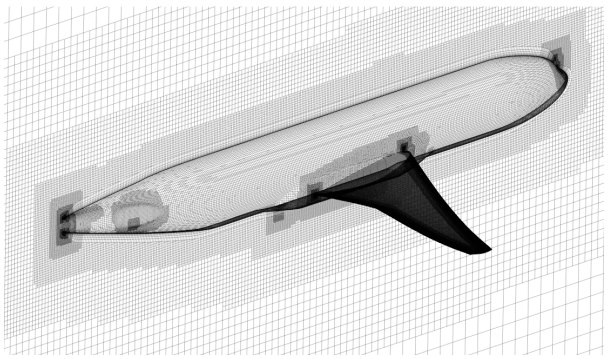

(c) Wing-Body (WB) mesh – $\mathcal{O}(24M)$ cells

Figure 3: CRM wing-body at $C_L = 0.5$, $M = 0.85$, $Re = 40M$

CRM nacelle inlet is oversized for this engine. As a consequence, spillage was higher than what is typically expected at cruise but deemed acceptable since the study is only considering relative changes.

The nominal CRM nacelle is asymmetric but, for convenience, it was modified to be symmetric such that the entire engine geometry, including the core, could be obtained by revolving the profile section shown in Fig. 4. The boundary conditions used to simulate the powered nacelle were a pressure-outlet condition at the fan-face and stagnation inlet conditions at the bypass and core nozzle plenums. As a verification, the isolated engine was simulated in CFD at cruise conditions of $M = 0.85$ and altitude of $10,668$ m with zero

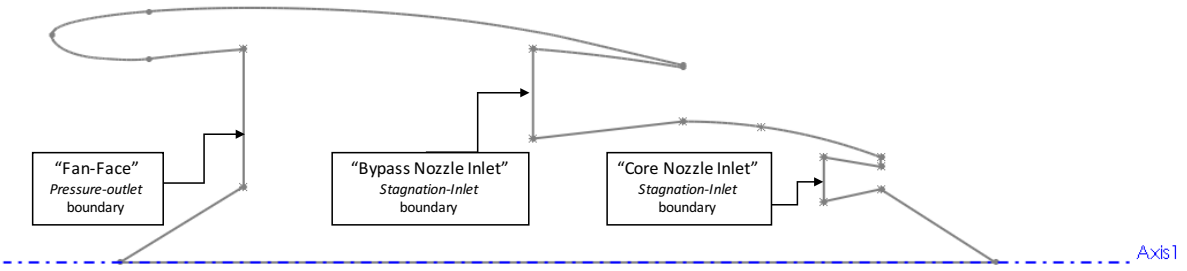

Figure 4: Powered nacelle boundary conditions

incidence angle and compared against EDS in in Table 3. Net thrust agreed within 10% which was deemed acceptable since a discrepancy between 3D RANS predictions and 1D cycle analysis is expected.

Table 3: Verification of RANS prediction of engine thrust

	EDS	CFD	Error(%)
Inlet massflow rate (lb/s)	1345.88	1502.79	10.44
Bypass nozzle massflow rate (lb/s)	1195.52	1143.352	-4.56
Core nozzle massflow rate (lb/s)	143.57	151.0188	4.93
Engine net thrust (lbf)	19,600	18,820	-4.14

V. Results

Sensitivity analysis results are presented in Fig. 5 using the method described in Section II, applied to each response. In the material to follow, the reader should interpret sensitivities in a relative sense, *i.e.* "relative to the effect of variable A, the effect of B is less (more) significant."

A. Airframe Installation Drag

The sensitivity analysis results for installation drag (ΔC_D) are shown in Fig. 5a. The magnitude of the bar indicates importance, while direction indicates whether the response increases or decreases with respect to that effect. The p-values are statistical measures of significance; smaller means more significant. The cutoff p-value was taken to be 0.05, meaning that all results are reported with 95% confidence. It can be seen that chord-wise placement (ΔX) is by far the most dominant effect. However, configuration type (TE/LE), and the interaction of configuration type with ΔX, ΔY, and ΔZ also influence the response with statistical significance. Each one will now be explained in more detail. No attempt was made to re-optimize airfoil shapes in this study; analysis holds for a fixed outer mold line.

1. *Effect of ΔX on ΔC_D*

The primary reason why this effect is so significant is that chord-wise placement drives the strength and location of the shock waves. This is known from previous work[12] and illustrated in Fig. 6 for two examples. Far away from the wing, interference effects essentially disappear; but close to it, the proximity of the nacelle causes local flow acceleration which results in stronger wave drag and even shock-induced boundary layer separation in some particularly bad cases.

2. *Effect of Configuration Type on ΔC_D*

Results show that placing the nacelle at the trailing edge is generally better than placing it at the LE. As shown in Fig. 6, the presence of the nacelle at TE locations creates back pressure that strengthens the primary shock on the wing and forces it to terminate early (compared to the clean wing), resulting in a loss of lift. At LE locations, the proximity of the nacelle causes local flow acceleration around the wing leading

Term	Contrast		Lenth t-Ratio	Individual p-Value
Δx	0.012462		22.51	<.0001*
TE/LE	0.001700		3.07	0.0123*
PC	-0.001144		-2.07	0.0520
Δy	-0.000309		-0.56	0.5891
Δz	-0.000124		-0.22	0.8226
Δx*Δx	0.001559	*	2.82	0.0182*
Δx*TE/LE	-0.000192		-0.35	0.7329
Δx*PC	-0.000309		-0.56	0.5891
TE/LE*PC	0.000296		0.53	0.6068
PC*PC	0.000037	*	0.07	0.9475
Δx*Δy	0.000490		0.89	0.3469
TE/LE*Δy	-0.002367		-4.27	0.0023*
PC*Δy	0.000139		0.25	0.8048
TE/LE*Δz	-0.001682		-3.04	0.0127*
PC*Δz	-0.000429	*	-0.77	0.4078
Δx*Δx*TE/LE	-0.002138	*	-3.86	0.0043*
Δx*TE/LE*PC	0.000789		1.42	0.1523
TE/LE*PC*PC	0.000062	*	0.11	0.9118
Δx*TE/LE*Δy	-0.000821		-1.48	0.1394
TE/LE*PC*Δy	0.000746		1.35	0.1699
TE/LE*PC*Δz	-0.000234	*	-0.42	0.6777

(a) Installation drag, ΔCD

Term	Contrast		Lenth t-Ratio	Individual p-Value
TE/LE	-0.514091		-4.70	0.0016*
Δz	-0.313195		-2.86	0.0167*
Δx	0.082615		0.76	0.4194
Δy	-0.080483		-0.74	0.4310
PC	0.073893		0.68	0.4708
TE/LE*Δz	0.311133		2.84	0.0174*
TE/LE*Δx	-0.071955		-0.66	0.5213
Δz*Δx	-0.069823	*	-0.64	0.5360
Δx*Δx	-0.243936	*	-2.23	0.0415*
TE/LE*Δy	0.069823		0.64	0.5360
Δz*Δy	0.069823	*	0.64	0.5360
Δx*Δy	-0.147641		-1.35	0.1690
TE/LE*PC	-0.070080		-0.64	0.5344
Δz*PC	0.106073	*	0.97	0.3052
PC*PC	-0.016002	*	-0.15	0.8841
TE/LE*Δz*Δx	0.067691	*	0.62	0.5492
TE/LE*Δx*Δx	0.249199	*	2.28	0.0378*
TE/LE*Δz*Δy	-0.067691	*	-0.62	0.5492
TE/LE*Δx*Δy	0.143377		1.31	0.1805
TE/LE*Δz*PC	-0.104166	*	-0.95	0.3126
TE/LE*PC*PC	0.003693	*	0.03	0.9747

(b) Pressure recovery, ΔPR

Term	Contrast		Lenth t-Ratio	Individual p-Value
TE/LE	0.080127		11.45	<.0001*
Δx	-0.028521		-4.08	0.0032*
Δy	0.007307		1.04	0.2745
PC	0.006217		0.89	0.3436
Δz	0.005858		0.84	0.3683
TE/LE*Δx	0.004930		0.70	0.4526
Δx*Δx	0.003999	*	0.57	0.5784
TE/LE*Δy	0.005623		0.80	0.3888
Δx*Δy	0.011721		1.68	0.1006
TE/LE*PC	-0.003642		-0.52	0.6135
Δx*PC	0.000965		0.14	0.8906
Δy*PC	0.007329		1.05	0.2732
PC*PC	0.000289	*	0.04	0.9674
TE/LE*Δz	-0.008487		-1.21	0.2113
PC*Δz	-0.000598	*	-0.09	0.9308
TE/LE*Δx*Δx	-0.017299	*	-2.47	0.0273*
TE/LE*Δx*Δy	0.002638		0.38	0.7129
TE/LE*Δx*PC	-0.001317		-0.19	0.8492
TE/LE*Δy*PC	0.004664		0.67	0.5002
TE/LE*PC*PC	0.000068	*	0.01	0.9936
TE/LE*PC*Δz	0.000527	*	0.08	0.9403

(c) Lift curve intercept, ΔC_{L_0}

Term	Contrast		Lenth t-Ratio	Individual p-Value
TE/LE	-0.016468		-7.60	0.0002*
Δx	-0.009599		-4.43	0.0021*
Δz	0.001475		0.68	0.4668
PC	0.001035		0.48	0.6393
Δy	-0.000645		-0.30	0.7674
TE/LE*Δx	-0.001317		-0.61	0.5566
Δx*Δx	0.001385	*	0.64	0.5346
TE/LE*Δz	0.004124		1.90	0.0681
Δx*Δz	-0.001924	*	-0.89	0.3439
TE/LE*PC	-0.001187		-0.55	0.5966
Δx*PC	0.001850		0.85	0.3610
Δz*PC	-0.004299	*	-1.98	0.0606
PC*PC	-0.000012	*	-0.01	0.9964
TE/LE*Δy	0.002137		0.99	0.2978
Δx*Δy	-0.002385	*	-1.10	0.2525
TE/LE*Δx*Δx	0.004685	*	2.16	0.0459*
TE/LE*Δx*Δz	-0.002489	*	-1.15	0.2334
TE/LE*Δx*PC	-0.001444		-0.67	0.5002
TE/LE*Δz*PC	-0.000383	*	-0.18	0.8608
TE/LE*PC*PC	-0.000062	*	-0.03	0.9796
TE/LE*Δx*Δy	-0.000200	*	-0.09	0.9247

(d) Lift curve slope, ΔC_{L_α}

Figure 5: Effect screening

edge, strengthening the primary shock and also causing it to terminate early with a similar loss of lift. In both cases, C_L must be maintained by increasing the angle of attack, resulting in higher leading-edge suction peak which is beneficial because it creates a component of force acting opposite to drag. Overall, OWN TE configurations seem to be inherently better at enhancing suction peak, while limiting wave drag penalties.

3. Effect of Power Code on ΔC_D

Results show that installation drag decreases as the engine power setting increases. This is because the engine ingests more air as power code goes up, which results in less "spillage" flow to interact with. However, this effect is not as prominent as the others; the p-value is only 0.520 compared to 0.0182 for the next highest. Hence, installation drag is weakly dependent on propulsion in comparison.

4. Interaction of ΔX and configuration type on ΔC_D

An interaction occurs when the setting of one factor changes the effect of another. For example, Fig. 7 shows that ΔC_D varies almost linearly with ΔX when the configuration is of LE type, but nonlinearly when it is

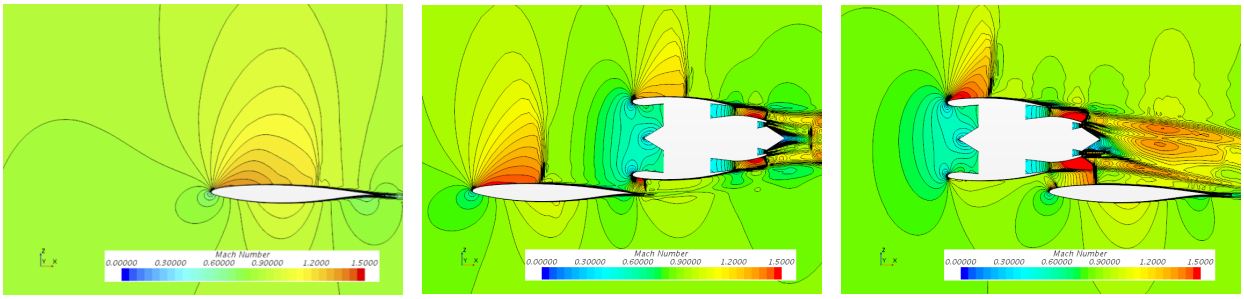

(a) Isolated wing-body (clean wing) (b) Trailing edge baseline (c) Leading edge baseline

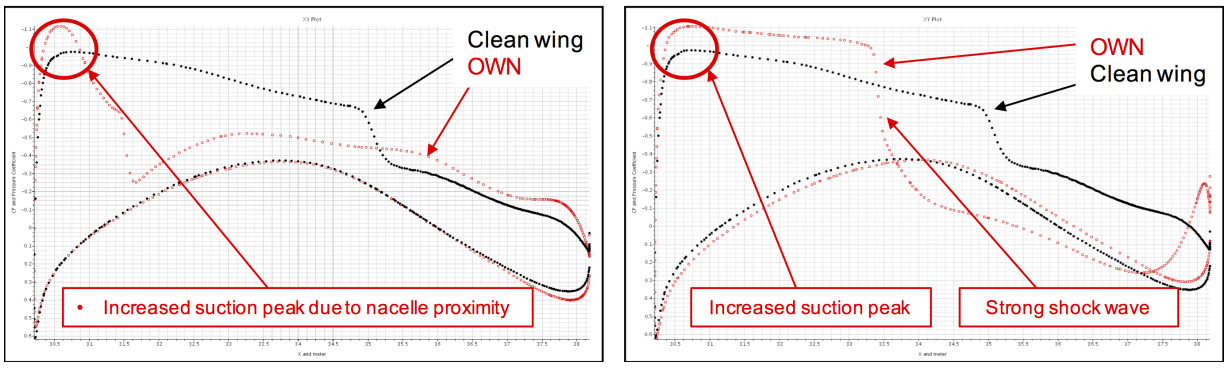

(d) Leading edge baseline Cp-distribution (e) Trailing edge baseline Cp-distribution

Figure 6: Mach contours and Cp-distribution at nacelle span location

of TE type. For LE configuration, the former suggests that installation drag is best reduced by placing the nacelle as far away as possible from the wing, whereas the latter suggests a point of diminishing return for TE configurations. This could imply the presence of a local optimum caused by some beneficial aerodynamic interaction when the inlet nacelle is close to the trailing edge. Although additional optimization would be needed to find out for certain, this trend supports the findings of others.[3,13]

5. Interaction of ΔY and configuration type on ΔC_D

At LE locations, installation drag decreases as the nacelle moves outboard as shown in Fig. 10b, but at TE locations it's the opposite as shown in Fig. 10a. This interaction is an unfortunate consequence of how the coordinate system was defined, as illustrated in Fig. 8. For LE configurations, the gap between the nacelle and the wing increases as the nacelle moves outboard due to leading-edge sweep, whereas for TE configurations it increases inboard. Therefore, the interaction between configuration type and ΔY is most likely just the manifestation of different effect: ΔX.

6. Interaction of ΔZ and configuration type on ΔC_D

At LE configurations, results suggests that installation drag decreases as the nacelle moves up and away from the wing; but at TE configurations, it's the opposite as shown in Fig. 7. However, in both cases the variation of ΔC_D with respect to ΔZ is within the noise of the regression model. Therefore, even though the interaction itself is statistically significant (change in sign), the factor it interacts with has negligible effect on the response and so it can be neglected too.

B. Engine Pressure Recovery

The sensitivity analysis results for "change in pressure recovery" (ΔPR) are shown in Fig. 5b. It can be seen that the dominating effects are configuration type (TE/LE), height above the wing ΔZ, and ΔX which has a strong nonlinear influence on the response. In addition, there exist statistically significant interactions between configuration type, ΔZ, and ΔX. Each one will now be explained in more detail.

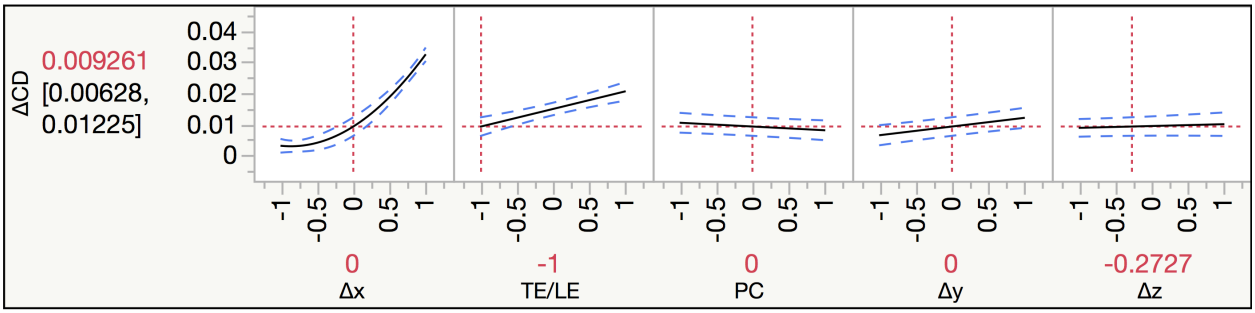

(a) Visualization of local profiles for TE configuration type

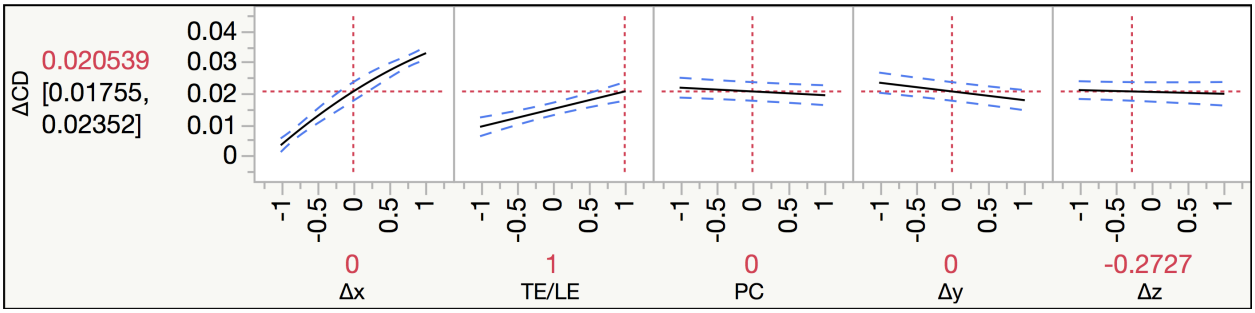

(b) Visualization of local profiles for LE configuration type

Figure 7: Local sensitivities analysis for ΔC_D response. *Each plot shows the local profile of the response along the dimension indicated. They correspond to the trace of the intersection between the response surface and the planes of a cartesian coordinate system whose origin lies at a point denoted by the dotted hairlines.*

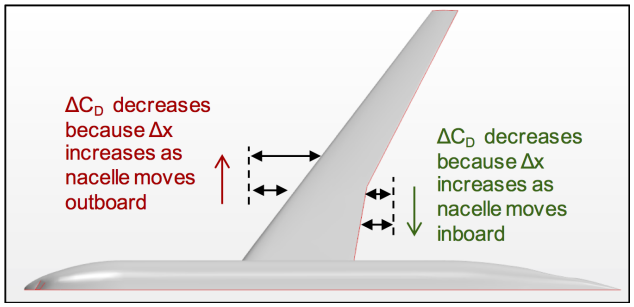

Figure 8: Interaction of "ΔY" and "config type" explained

1. *Effect of configuration type on* ΔPR

Fig. 5b shows that pressure recovery decreases (*i.e.* ΔPR is non-zero) when the nacelle is placed at TE locations. This is because the flow entering the nacelle is non-isentropic at those locations; *i.e.* there is a strong shock on the wing ahead of the inlet, as shown Fig. 6b. This implies a strong dependence of propulsive efficiency on airframe aerodynamics and, as a result, there is a tradeoff between *good* installation drag and *poor* pressure recovery at TE locations. This is significant because a 2% loss in pressure recovery translates into a 9% loss in fuel burn for a representative civil transport, as shown in Fig. 9.

2. *Effect of* ΔZ *and configuration type on* ΔPR

Fig. 5b shows that pressure recovery decreases as the engine moves closer to the wing; but this trend only occurs at TE nacelle locations, as shown in Fig. 10. Again, this implies a strong dependence of propulsion efficiency on airframe aerodynamics for TE configurations only. The trend itself makes intuitive sense, since moving the engine away from wing reduces interference and, therefore, pressure recovery losses.

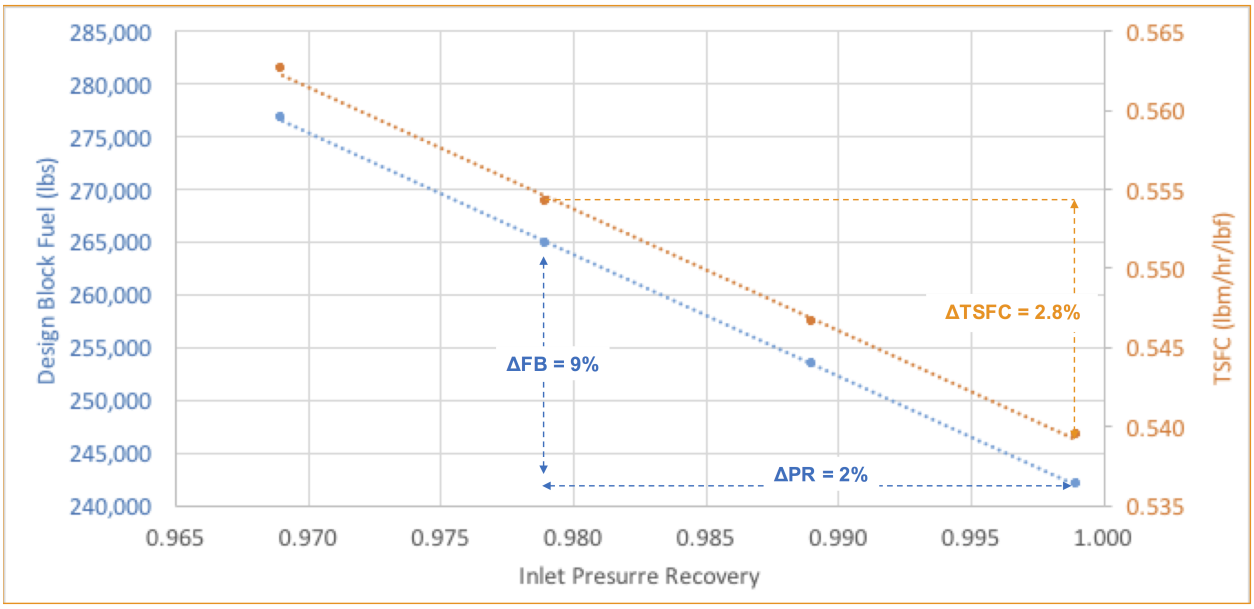

Figure 9: Fuel burn as a function of pressure recovery for a notional 300 passenger class transport and high bypass 94,000 lbs thrust class turbofans (generated using EDS[11])

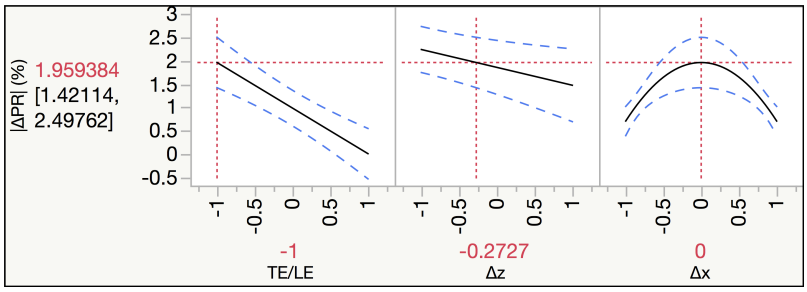

(a) Visualization of local profiles for TE configuration type

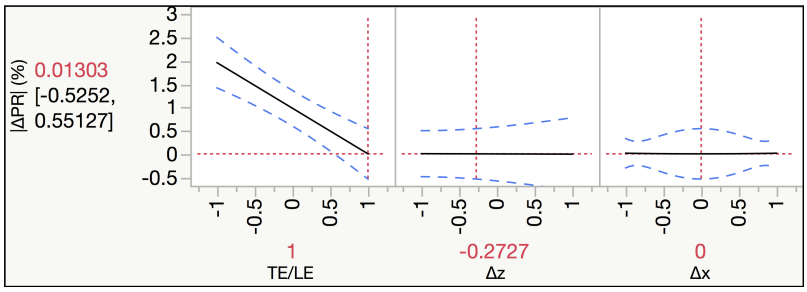

(b) Visualization of local profiles for LE configuration type

Figure 10: Local sensitivities analysis for ΔPR response

3. *Effect of ΔX and configuration type on ΔPR*

Fig. 10 shows that pressure recovery is a nonlinear function of ΔX; but only at TE nacelle locations. This nonlinearity can be explained by taking a look at Fig. 11, which shows the Mach contours for three different TE configurations: $-\Delta X$, baseline, and $+\Delta X$. It can be seen ΔPR is largest for the TE baseline, which coincides with the case where the primary shock on the wing (ahead of the inlet) is strongest. Although this study did not conduct any shape optimization, this result suggests that pressure recovery will be particularly

sensitive to how well the wing design is able to weaken the shock. Again, this is evidence of strong dependence between propulsive efficiency and aerodynamic design.

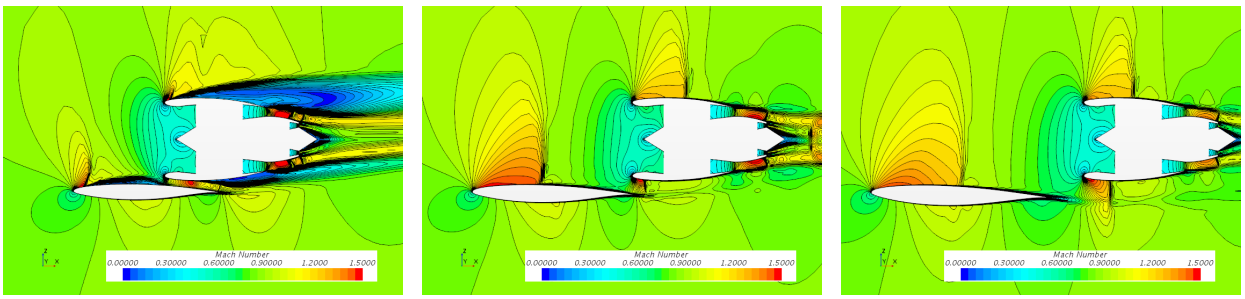

(a) Treatment 10: $\Delta PR = -0.39\%$ (b) TE Baseline: $\Delta PR = -2.5\%$ (c) Treatment 8: $\Delta PR = -0.38\%$

Figure 11: Mach contours at nacelle span location

C. Lift Curve

The sensitivity analysis results of the lift curve parameters are shown in Figs. 5c and 5d. It can be seen that the dominating effects are configuration type (TE/LE) and ΔX, which will now be discussed in detail.

1. *Effect of configuration type on* ΔC_{L_α} *and* ΔC_{L_0}

To better interpret the sensitivity analysis of Figs. 5c and 5d, consider Fig. 12 which shows how the lift curve changes for TE/LE configurations compared to the clean wing. For LE configurations, the lift curve intercept (C_{L_0}) increases and the lift curve slope (C_{L_α}) decreases, which is expected due to the Coandă effect. As the jet exhaust blows over the surface of the wing, it enhances the circulation which contributes to lift. Sensitivity with respect to angle of attack therefore decreases because circulation is now partly dependent on the engine, not just the wing. For TE configuration, C_{L_0} drops significantly because the presence of the engine creates back pressure on the wing, which effectively dumps lift.

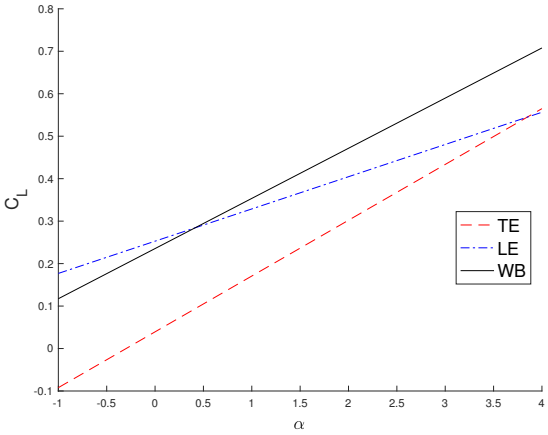

Figure 12: Change in lift due to configuration type

2. *Effect of* ΔX *on* ΔC_{L_α} *and* ΔC_{L_0}

For LE configurations, there is a powered lift benefit due to the jet blowing over the wing, but this benefit erodes quickly if the nacelle moves towards the wing (*i.e.* positive ΔX), as shown in Fig. 13a. In fact, the convexity of the profile suggests that there is a maximum. Hence, in general, the nacelle must be close but not close to take advantage of powered lift when the configuration is of LE type. However, for TE

configurations, the trend and curvature of the profiles are reversed: moving away from the wing is generally better for preserving the lift properties of the clean wing.

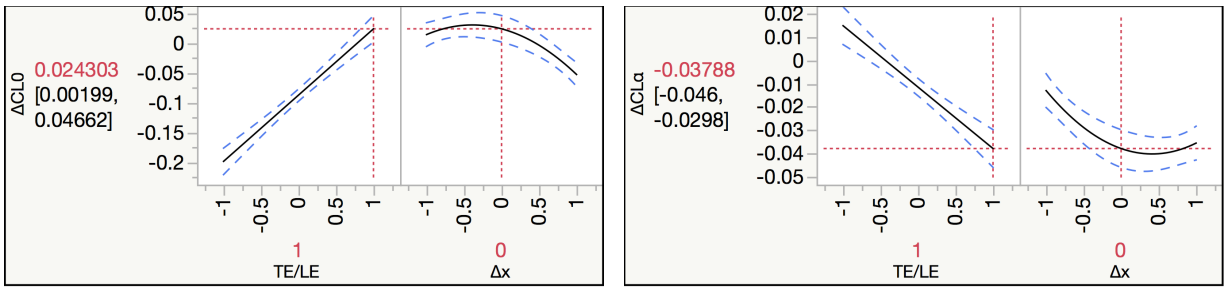

(a) Intercept *vs.* ΔX when config type = LE

(b) Slope *vs.* ΔX when config type = LE

(c) Intercept *vs.* ΔX when config type = TE

(d) Slope *vs.* ΔX when config type = TE

Figure 13: Local sensitivity analysis of lift curve parameters

Table 4: Summary of significant OWN variables

Description	C_{L_α}	C_{L_0}	C_D	PR
Config Type	✓	✓	✓	✓
ΔX	✓	✓	✓	✓
ΔZ				✓
Power Code			✓	

VI. Conclusion

This study conducted a sensitivity analysis of installation drag, pressure recovery, and lift curve parameters for podded OWN concepts with respect to the following design variables: XYZ nacelle location, configuration type (TE or LE), and engine power setting. A summary of the most significant variables per response is provided in Table 4. It was found that the aerodynamic and propulsion disciplines are weakly coupled: engine pressure recovery is strongly affected by airframe aerodynamics when the nacelle is placed at the trailing edge and, in return, installation drag is weakly affected by the engine's power setting, especially at TE configurations. OWN therefore represents a weakly coupled, multi-disciplinary system which requires a coupled MDA modeling and simulation approach, as illustrated in Fig. 1. Furthermore, it was observed that there is a tradeoff between installation drag and pressure recovery for TE configurations: the *best* nacelle location for installation drag was also found to be the *worst* for pressure recovery. Aerodynamic benefits should thus be carefully traded with propulsion penalties in order to assess the fuel burn potential of OWN concepts. Finally, this study was limited by the use of a fixed outer mold line. Future work should consider re-optimizing the nacelle for each DOE case. The authors expect that overall trends would remain, but that the relative sensitivity of ΔC_D due to ΔX would decrease, while that of due to power setting would increase.

References

[1]Gray, J. S., Mader, C. A., Kenway, G. K., and Martins, J., "Approach to Modeling Boundary Layer Ingestion using a Fully Coupled Propulsion-RANS Model," *58th AIAA/ASCE/AHS/ASC Structures, Structural Dynamics, and Materials Conference*, AIAA SciTech Forum, American Institute of Aeronautics and Astronautics, jan 2017.

[2]Wimpress, J. K. and Newberry, C. F., *The YC-14 STOL Prototype: Its Design, Development, and Flight Test An Engineer's Personal View of an Airplane Development*, AIAA, 1998.

[3]Hooker, J. R., Wick, A., Zeune, C. H., and Agelastos, A., "Over Wing Nacelle Installations for Improved Energy Efficiency," *31st AIAA Applied Aerodynamics Conference*, 2013.

[4]Vassberg, J., Dehaan, M., Rivers, M., and Wahls, R., "Development of a Common Research Model for Applied CFD Validation Studies," *26th AIAA Applied Aerodynamics Conference*, , No. August, 2008, pp. 1–22.

[5]Hines, W. W., Montgomery, D. C., Goldsman, D. M., and Borror, C. M., *Probability and Statistics in Engineering*, Wiley, 2003.

[6]Myer, R. and Montgomery, D., *Response Surface Methodology: Process and Product Optimization Using Designed Experiments*, Wiley, 2002.

[7]Russell V. Lenth, "No Title," *Technometrics*, Vol. 31, No. 4, 1989, pp. 469–473.

[8]Raymond H. Myers, Douglas C. Montgomery, and Anderson-Cook, C. M., *Response Surface Methodology*, Wiley, John Wiley & Sons Inc., New York, 2nd ed., 2009.

[9]Plackett, R. L. and Burman, J. P., "The Design of Optimum Multifactorial Experiments," *Biometrika*, Vol. 33, No. 4, 1946, pp. 305.

[10]Taylor, N., Gammon, M., and Vassberg, J., "The NASA Common Research Model: a Geometry Handling Perspective," *46th AIAA Fluid Dynamics Conference*, 2016.

[11]Kirby, M. and Mavris, D., "The Environmental Design Space," *26th International Congress of the Aeronautical Sciences*, Anchorage, Alaska, 14 - 19 September 2008.

[12]Berguin, S. H., *A method for reducing dimensionality in large design problems with computationally expensive analyses*, Ph.D. thesis, Georgia Institute of Technology, 2015, pp. 16 – 37.

[13]Fujino, M. and Kawamura, Y., "Wave-Drag Characteristics of an Over-the-Wing Nacelle Business-Jet Configuration," *41st Aerospace Sciences Meeting and Exhibit*, , No. January, 2003, pp. 1–11.